

Review of channel models for deep space communications

Xiaohan PAN, Yafeng ZHAN*, Peng WAN & Jianhua LU

Space Center, Tsinghua University, Beijing 100084, China

Received 13 September 2017/Revised 5 December 2017/Accepted 23 January 2018/Published online 7 March 2018

Abstract This paper presents a comprehensive review of channel models for deep space communications. Based on the characteristics of environment, deep space channels can be divided into three kinds, i.e., near Earth link, interstellar link and near planet link. The modeling for different kinds of channels are summarized respectively, and some simulation results are provided in this paper. In addition, according to the development trend of deep space communications, optical wave will become an important carrier in the future. Therefore, deep space optical communication is also briefly introduced. Finally, challenges of deep space channel modeling are pointed out and future research direction is also discussed.

Keywords deep space communication, channel modeling, microwave communication, optical communication, deep space exploration

Citation Pan X H, Zhan Y F, Wan P, et al. Review of channel models for deep space communications. *Sci China Inf Sci*, 2018, 61(4): 040304, <https://doi.org/10.1007/s11432-017-9345-8>

1 Introduction

In deep space exploration mission, reliable communication system plays the guaranteeing role in the success of whole task. Data transmission, tracking, navigation, telemetry and telecommand are all depended on this system. As an important part of communication system, channel is the base to research system performance and various signal-processing algorithms. In this case, channel modeling is significantly important.

In comparison with mobile communication and general satellite communication, deep space communication has significantly different characteristics [1]. First, the communication distance is far and the signal attenuation is large. The average distance from the Earth to the Moon is about 380000 km, and to Pluto is as high as 4.4 billion to 7.4 billion kilometers. Such long distance will arise a great attenuation during transmission, and the SNR of received signal is extremely low. Second, the transmission delay is very large and unstable. It takes few seconds to communicate with the Moon probe, but few hours with Pluto probe, and the delay varies under different circumstances. The duration of each communication may even be less than the signal transmission. Third, the communication link is intermittent. Due to the rotation and revolution of the planets, links are often interrupted. In addition, the existence of various cosmic rays can disturb the useful signal during transmission process, resulting in random interruption. Fourth, the uplink and downlink are asymmetric. Channel capacity and transmission data rate are different, and sometimes there is only one-way channel. Additionally, the capacity of the spacecraft makes the

* Corresponding author (email: zhanyf@tsinghua.edu.cn)

payload volume, weight and complexity limited, which leads to a lot of technical constraints. Therefore, there exists a great deal of challenges for deep space communications.

Great effort has been devoted to channel models for deep space communications. In traditional research, the channel is usually regarded as an ideal additive white gaussian noise channel (AWGN), which shows a large deviation from the actual situation. Then the variable parameter AWGN channel (VPAWGN) appeared, which is more accurate [2], but did not take the impact of solar scintillation into consideration yet. From the 1970s, the National Aeronautics and Space Administration (NASA) carried out a series of deep space exploration missions to study the performance of deep space communication links and obtained a large number of observations [3–7]. Based on these data, Ferial et al. [8] established an amplitude fluctuation model for free space, but only considered the effect of weak solar scintillation. Morabito [9] found a relationship between the scintillation index and the Rician factor, and established a Rician channel model for deep space communications. Since then, the Rician channel model has been constantly improved. Sun-Earth-probe angle (SEP) has been considered and the widely used in variable parameters Rician channel model (VPRician) [10]. Although research on deep space channel model has been conducting, different factors have to be considered under different scenarios such as near-Earth orbit, transfer orbit, Entry-Descent-Landing (EDL) orbit. As a result, the channel modeling method must change and it is difficult to find a unified model. Recently, though some valuable efforts have been made on deep space link division, the theoretical model is too simple and incomplete [11, 12]. Therefore, it is essential to classify and research the channel characters in different deep space environments.

In this paper, deep space communication channel is classified into three kinds and existing modeling methods are introduced under different scenarios. Besides, some simulation results are given. In addition, with the development of technologies, optical wave will become an important carrier in the future. Therefore, this paper will also briefly introduce the characteristics of deep space optical communication and its channel modeling. Finally, challenges and future research direction are pointed out.

2 Deep space microwave communication channel

Space communication can be divided into near space communication and deep space communication, which has a distance boundary of 2×10^6 km away from the Earth [13]. Figure 1 shows a diagram of deep space communication link which takes Mars as an example. In deep space communication system, we can divide the channel link into three parts: near Earth link, interstellar link and near planet link. Different links are subject to different interference and noise, so it is necessary to introduce channel modeling method according to the characteristics of each link.

2.1 Near Earth link

Main interference in near Earth link comes from the Earth's atmosphere. The atmosphere will bring about atmospheric losses, rain and fog losses [14, 15].

- **Atmospheric loss.** Atmospheric loss is reflected in atmospheric absorption and atmospheric scintillation. Atmospheric absorption means the electromagnetic wave will be absorbed by electrons, water vapor molecules and oxygen molecules when it propagates through the atmosphere. The attenuation is related to distance which can be calculated as follows:

$$\Gamma_A = \int_0^{r_0} (\gamma_0(r) + \gamma_w(r)) dr \quad (\text{dB}), \quad (1)$$

where $\gamma_0(r)$ is the propagation distance (km), $\gamma_0(r)$ and $\gamma_w(r)$ are the loss rate of oxygen molecules and water vapor molecules, respectively, whose impact can be basically ignored in 0.3–10 GHz frequency band. In the transmission path, the tropospheric atmospheric turbulence causes change of atmospheric refractive index, so atmospheric scintillation comes about. It will make the amplitude and phase of received signal fluctuate. Many statistical models have been established to describe atmospheric scintillation: STHV2 model, ITU-R model, Ortgies-N model, Karasawa model and van de Kamp model, while van de Kamp

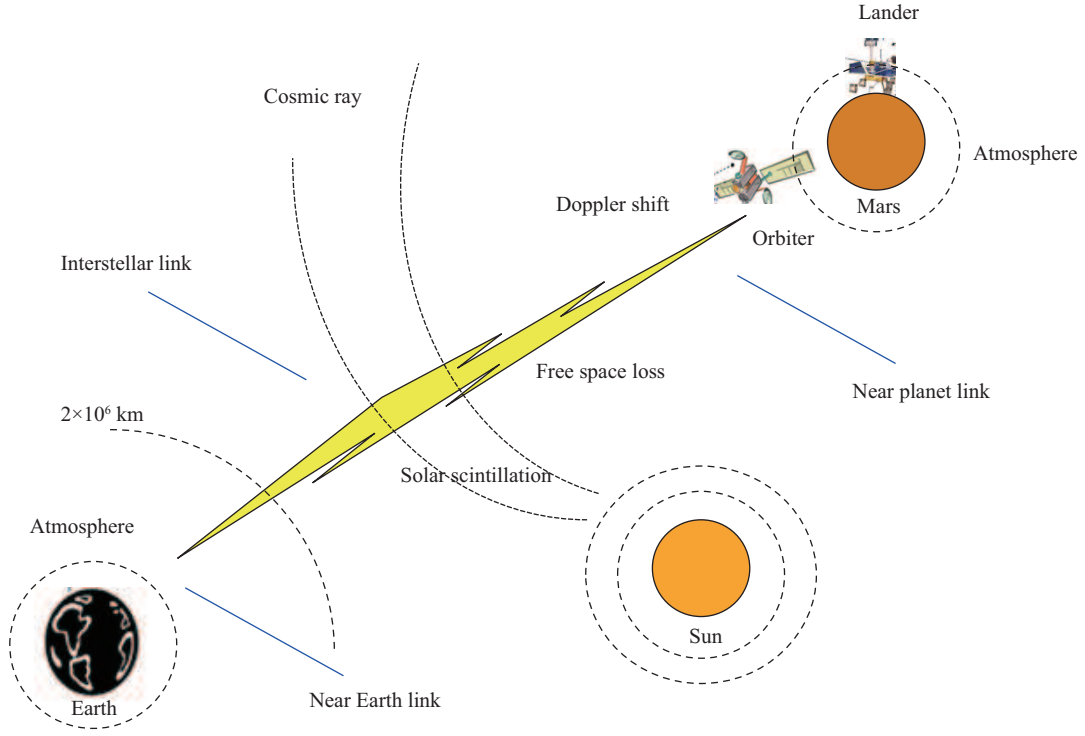


Figure 1 (Color online) A diagram of deep space communication link.

model is the latest improved one. It only needs some meteorological information. The standard deviation can be expressed as

$$\sigma_x = \sigma_{r0} f^{7/12} g(x) / (\sin \theta)^{6/5}, \quad (2)$$

where $\sigma_{r0} = 3.6 \times 10^{-3} + 1.03 \times 10^{-4} N_{\text{wet}}$, N_{wet} is the wet term refractive index, and $g(x)$ is the antenna average function.

- Rain and fog loss. Rain and fog loss has two parts: rain attenuation, cloud and fog attenuation. Rain attenuation mainly comes from the scattering absorption of rains whose specific attenuation is related to regional precipitation. It can be calculated with the attenuation coefficient of unit path length [16, 17],

$$r_R = 4.343 \times 10^3 \times \int_0^\infty n(a_r) Q(a_r, \lambda) da_r, \quad (3)$$

where a_r is the raindrop radius, $n(a_r)$ is the number of rain drops per unit volume, and $Q(a_r, \lambda)$ is the attenuation cross-sectional area. Cloud and fog attenuation is generally calculated according to the ground-to-air path attenuation formula proposed by international telecommunication union radio (ITU-R)

$$A_c = \frac{LK_1}{\sin \theta}, \quad (4)$$

where L is the total columnar liquid water content, K_1 is the attenuation coefficient, and θ is the elevation angle. In different weather conditions, the channel characteristics vary, so the attenuation will also change. In cloudy weather, due to the large amount of clouds, there will be multipath and shadow effects, so it can be described by Corazza model [18], which is composed of Rician distribution and Lognormal distribution. And in foggy weather, fog concentration is the factor that mainly determines the attenuation of signal. Therefore, it can be described by Nakagami model whose fading factor p represents the concentration of fog [19, 20]. The larger the concentration is, the smaller p values.

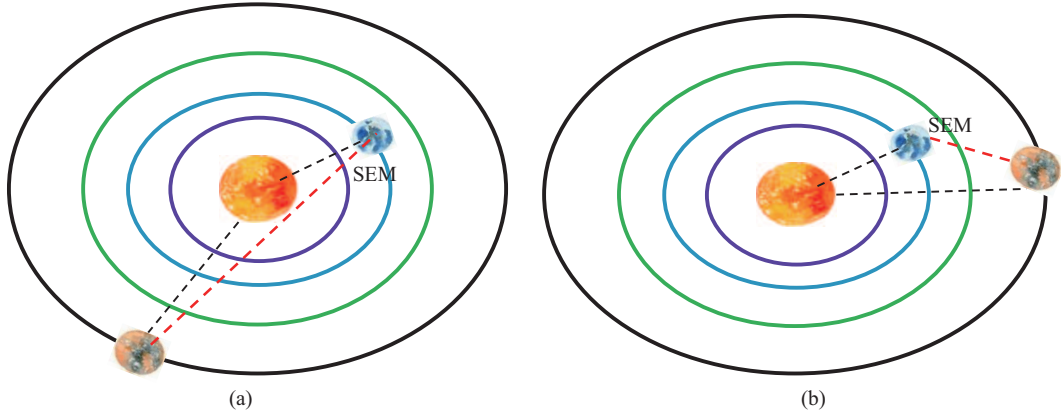


Figure 2 (Color online) (a) Superior conjunction; (b) inferior conjunction.

2.2 Interstellar link

2.2.1 Link model

- Free-space loss. Interstellar link is the most important link in deep space communication, which is characterized by very long transmission distance. So the main attenuation in this link comes from free-space attenuation

$$L_{bs} \approx 32.45 + 20\lg f + 20\lg d, \quad (5)$$

where f is frequency (MHz), and d is distance (km). For deep space communication, f is usually in X (8–12 GHz), Ka (27–40 GHz) and other bands.

- Solar scintillation. Solar scintillation is a kind of important interference in deep space communication, and it is also the focus of research. When deep space probe arrives near the Sun, the electromagnetic waves are scattered through the charged particles from the Sun, resulting in multipath effect. From the 1970s, NASA began to explore the impact of solar scintillation. Morabito found a relationship between scintillation index and Rician factor in 2003, and established the Rician channel model. Until now the study of Rician model has been gradually improved [8, 21–24].

We use index m to measure the intensity of solar scintillation which expresses plasma density in the solar wind. It is weak scintillation when $m < 0.3$, transition zone when $0.3 < m < 1$, while strong scintillation when $m = 1$. The relationship between Rician factor and m can be expressed as

$$\gamma = \frac{\sqrt{1 - m^2}}{1 - \sqrt{1 - m^2}}. \quad (6)$$

In planetary revolution, there is a special state called solar conjunction, which can be described with the SEP angle. Two kinds of spatial location are shown in Figure 2.

It can be seen that when the planets are near superior conjunction, the communication link is very close to the Sun and is significantly disturbed by solar scintillation. On the contrary when the planets are near inferior conjunction, the communication link is far from the Sun and less disturbed. The relationship between scintillation index m and SEP angle in X-band has been observed by NASA. Please refer to Figure 2 in [25].

According to the curve, a fitting expression of SEP- m is given [26],

$$m = \begin{cases} e^{-a_1(\text{SEP} - \theta_0) + a_2(\text{SEP} - \theta_0)}, & \text{SEP} < \theta_0, \\ 1, & \text{SEP} > \theta_0, \end{cases} \quad (7)$$

where $a_1 = 1.14 \pm 0.09$, $a_2 = 0.02 \pm 0.02$ and θ_0 is about -1.3 degree.

Figure 3 shows the simulation results about the influence of different solar scintillation indexes on signal. As can be seen from the figure, solar scintillation impact on the signal increases with increasing index m . When m is equal to 1, it reaches a strong scintillation state. In actual communication link, the solar scintillation has less influence and m is about zero in most cases.

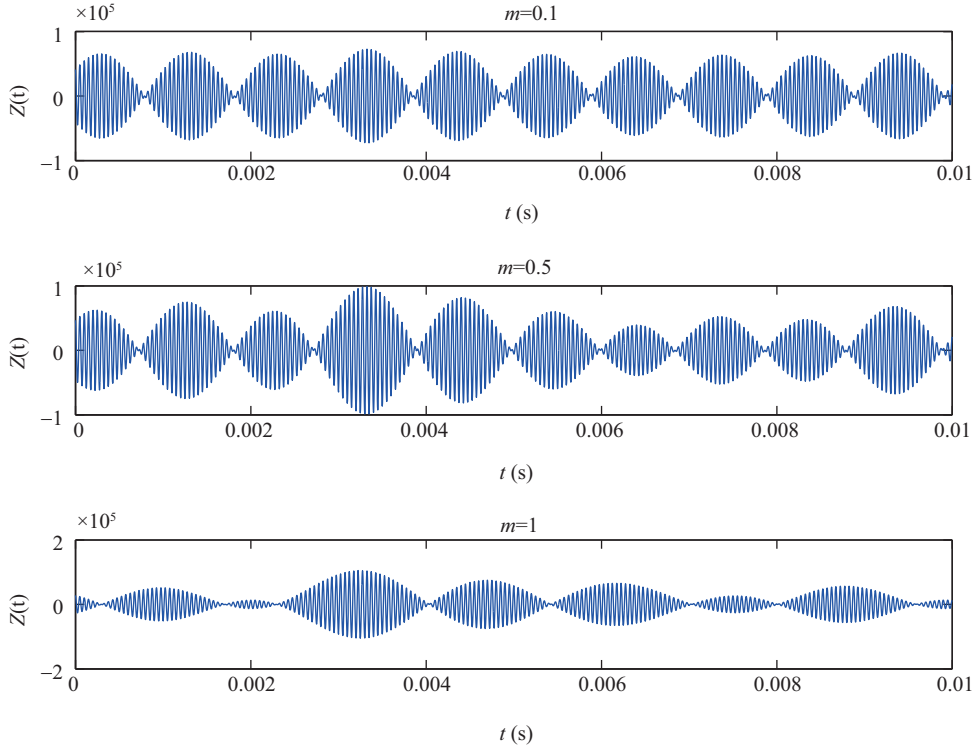


Figure 3 (Color online) Influence of solar scintillation index on signal.

- Antenna loss. Antenna loss is divided into two parts: the antenna pointing error loss and the antenna polarization error loss. In actual scene, pointing error loss is caused due to the spindle axis of receiving antenna cannot accurately point to the maximum gain direction of transmitting antenna. For spaceborne and ground station antenna, the cause of error is different. The former is determined by control accuracy, while the latter is determined by rotation accuracy and weather conditions. Relationship between actual gain of the antenna and the pointing error is as follows [27]:

$$G(\theta) = G_m e^{-2.77(\theta/\theta_{0.5})^2}, \quad (8)$$

where G_m is the maximum gain of antenna, $\theta_{0.5}$ is the beam width, and θ is the antenna pointing error. Therefore the pointing loss can be expressed as follows:

$$[L_{pe}] = [G_m] - [G(\theta)] = 12(\theta/\theta_{0.5})^2. \quad (9)$$

The antenna polarization loss is caused by the satellite altitude changes which make the transceiver antenna cannot realize polarization matching. The calculation expression is

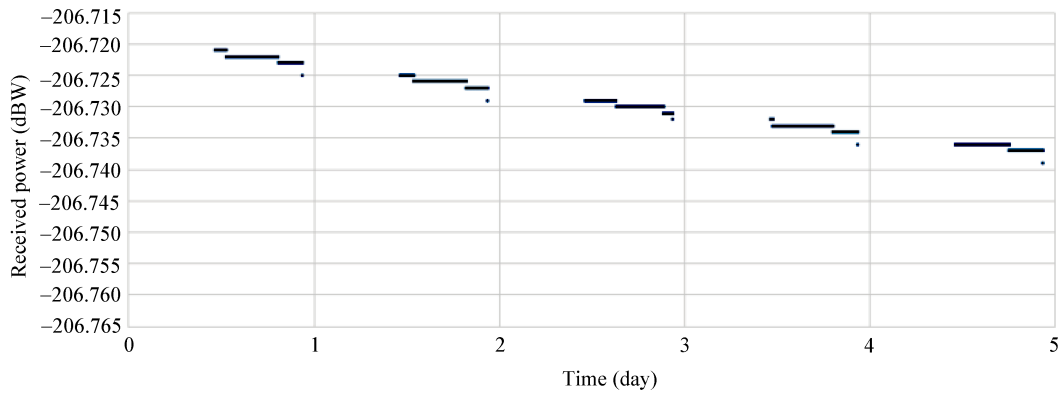
$$L_p = -10 \lg \frac{1}{2} \left[1 + \frac{\pm 4X_T X_R + (1 - X_T^2)(1 - X_R^2) \cos 2a}{(1 + X_T^2)(1 + X_R^2)} \right], \quad (10)$$

where X_T is the ratio of long axis to minor axis of the receiving electromagnetic wave, X_R is the axis ratio of receiving system, and a is the long axis angle of the transmitting and receiving electromagnetic waves. When the polarization direction of electromagnetic wave coincides with the system, the sign is positive. Otherwise it is negative.

- Cosmic ray interference. In addition, there are complex cosmic rays in interstellar links, which come from the outer solar system. At present, when analyzing the channel model, it is usually considered to be cosmic noise that obeys the Gaussian distribution and has flat power spectral density.

Table 1 Ground station, orbiter and Mars rover parameter settings

Ground station	Orbiter	Mars rover
Longitude 58.67° W	Semi-major axis 9509.57 km	Longitude 48.222° W
Latitude 34.59° S	Eccentricity 0.615	Latitude 22.697° N
Altitude 0.0	Inclination 86.9	Altitude 0.0
Antenna aperture 35 m	Transmitter power 44.3 dBW	Received frequency 415 MHz
Received frequency 8.5 GHz	Frequency (ground) 8.5 GHz	Bandwidth 2 MHz
Bandwidth 2 MHz	Frequency (rover) 415 MHz	G/T -20.0 dB/k
Antenna efficiency 50%	Antenna aperture 2.5 m	
	Antenna efficiency 50%	

**Figure 4** (Color online) Received power of the ground station from Mars orbiter.

2.2.2 Simulation

According to the above analysis, we use STK (system tool kit) software to simulate the ground station-orbiter link and the orbiter-Mars rover link with a background of the future Mars exploration project. The parameters are shown in Table 1. The simulation time is set from March 2021 to April 2021.

The simulation results of received power attenuation, on-off characteristics, Doppler shift and solar scintillation index of the ground station-orbiter link and the orbiter-Mars rover link are as follows.

Figures 4 and 5 show the received power of the ground station and the Mars orbiter in 5 days. As shown in Figure 4, the received power of ground station is decreasing and relatively stable, so we can know the Earth and Mars are gradually moving away from each other at the simulation time. The reason of keeping stable is that the distance between the Earth and Mars is very far and the relative distance change has little effect. While for the Mars orbiter shown in Figure 5, the impact of the relative distance change is very large, so the fluctuation of received power is also large. Moreover, there are some discrete points in Figure 5, which are caused by the rapid drift of the orbiter at periareon, and the duration is very short, which is not suitable for communication.

Figures 6 and 7 show on-off characteristics of the links. The visible time ratio of these two links is about 40% and 30%. Moreover, the ground station-orbiter link is relatively stable, while the orbiter-Mars rover link is more disorderly. Simulation results of specific loss, Doppler shift and solar scintillation coefficient are shown in Table 2.

2.3 Near planet link

Analysis of the near planet link can be analogous to the near Earth link, whose most important disturbance is also the atmosphere. The difference is that atmospheric conditions vary. The atmosphere of Mars is thin and the attenuation of electromagnetic waves, which is almost negligible, is much smaller than the Earth [28]. And the atmosphere of Pluto only exists in the form of gas at perihelion while in the rest of time it is condensed into solid. So we can choose a communication time to avoid atmospheric interference. In addition, some planets will have dust on the surface which is considered to be able to

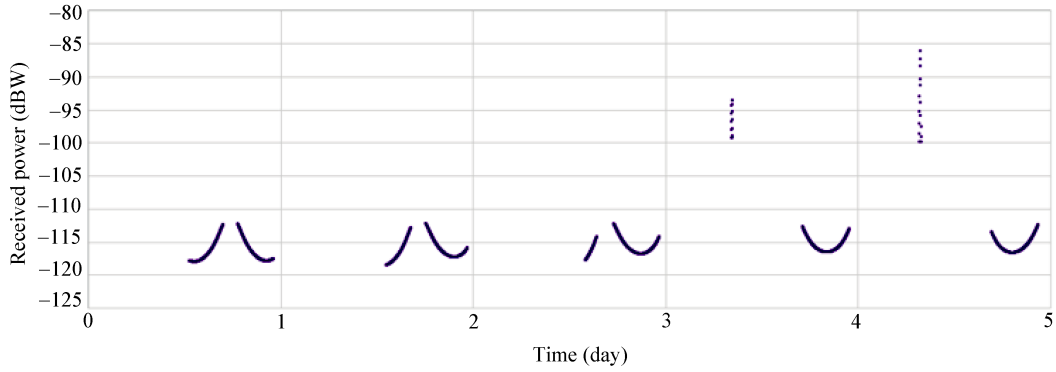


Figure 5 (Color online) Received power of the Mars orbiter from Mars rover.

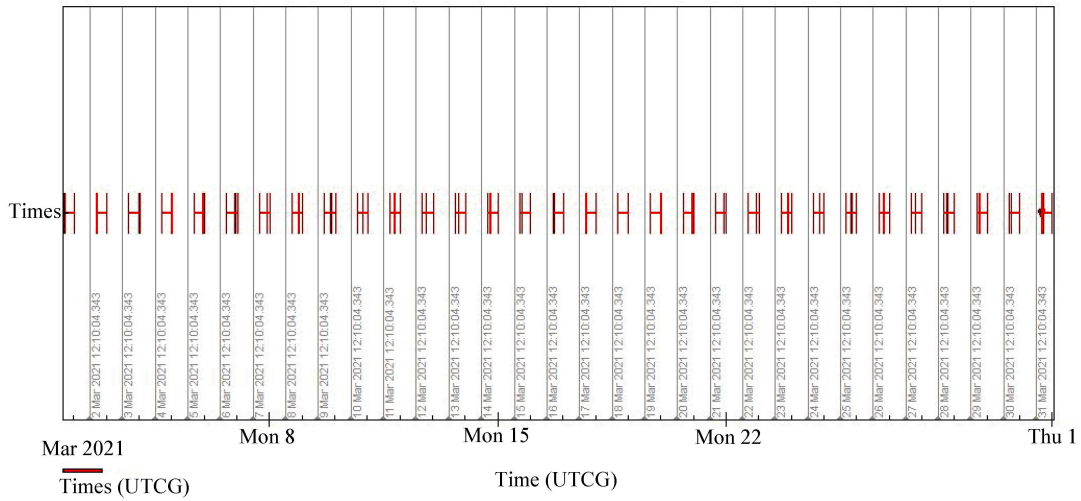


Figure 6 (Color online) Visible time of the ground station-orbiter link.

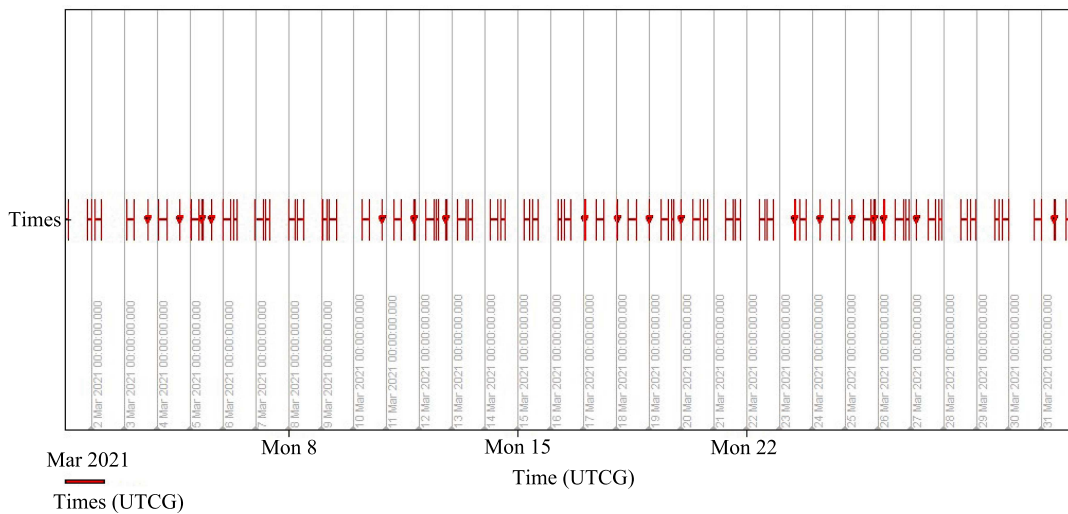


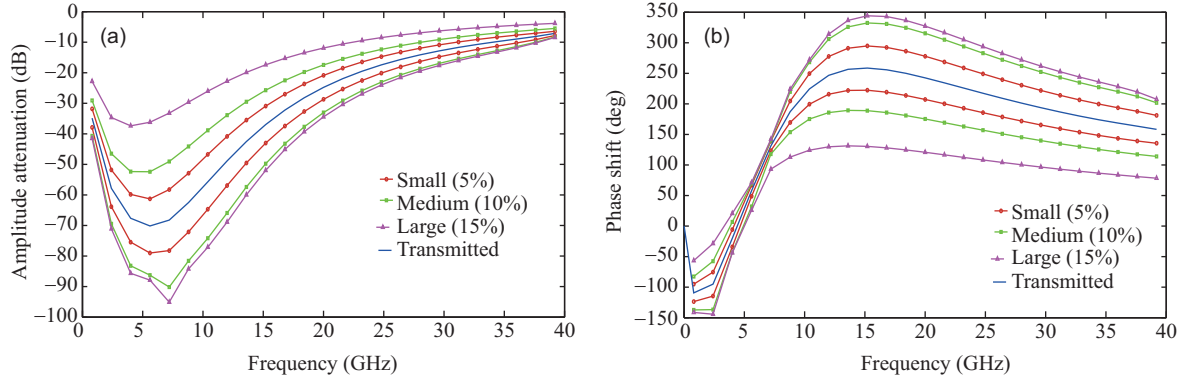
Figure 7 (Color online) Visible time of the orbiter-Mars rover link.

interrupt the communication. In the actual design of channel link, it is recommended to leave a certain electrical level allowance.

There is a special channel in the EDL stage when the atmosphere exists, called the plasma sheath channel. When a spacecraft enters the atmosphere, the tremendous heat generated by atmospheric

Table 2 Simulation results list

	Ground station–orbiter	Orbiter–Mars rover
Transmitter power (dBW)	44.3	44.3
Transmitter gain (dBW)	43.9432	17.716
EIRP (dBW)	88.243	62.016
Receiver gain (dBW)	66.825	62.016
Distance (km)	$[2.2, 2.6] \times 10^8$	[359.69, 14973.93]
Doppler shift (kHz)	[-386, -567]	[-5.30, 5.59]
Free-space loss (dB)	[-277.8, -279.4]	[-168.31, -135.92]
Atmosphere loss (dB)	[-0.07, 0.29]	0
Antenna pointing loss (dB)	$-(2.296 + 0.3)$	-2.296
Rain attenuation (dB)	[-1.3, -4.4]	0
Cosmic ray loss (dB)	[-0.0417, -0.3173]	0
Scintillation index m	[0, 0.3]	0

**Figure 8** (Color online) (a) Amplitude attenuation and (b) phase shift caused by the plasma sheath at a speed of 6000 m/s.

frictions makes the surrounding air ionize and forms a plasma sheath wrapped on the surface of the spacecraft. It can cause significant attenuation and large dynamic dithering of electromagnetic waves, which seriously affects the performance of communication. The Mars Pathfinder in 1997 and the Curiosity Rover in 2012 both suffered signal interruption for seconds. Figure 4 in [29] shows the change of received signal level during the landing of the Curiosity, where the level fluctuation reaches a maximum of 30 dB [29–31].

This phenomenon cannot be effectively overcome in the actual project at present and the received signal will have a brief interruption. For this reason, a space-time perturbation model of plasma sheaths electron density has been established [32–34],

$$n_e(x, t) = T\{n_0(x)\} \times [1 + \Delta \cdot n(t)], \quad (11)$$

where $n_0(x)$ is the steady state distribution of plasma sheaths, Δ is the relative turbulence intensity and $T\{\}$ represents turbulent mapping. According to this model, the influence on electromagnetic wave transmission of the sheath channel can be simulated [35].

Figure 8 shows the amplitude attenuation and phase shift caused by the plasma sheath. The blue curve represents results in the steady state, and the others represent the upper and lower bounds of possible fluctuation under different turbulence intensity.

3 Deep space optical communication channel

With the need for faster transmission rates and greater communication capacity in deep space exploration, traditional microwave communication has become increasingly difficult to meet the requirements of deep

space communication, so wireless optical communication was born. Optical communication has the characteristics of narrow beam width, large capacity, small delay and high confidentiality. It is considered as an important development direction to realize high speed communication. The time of researches on optical communication is more than 40 years [36–41]. NASA successfully carried out space optical communication in 2014 with a video transmission rate of 50 Mbps from the international space station to the Earth, which only takes 3.5 s while traditional downlink mode will take more than 10 min. This means that the optical communication will soon realize engineering applications. This section briefly describes channel modeling of spatial optical communication, including the transmission attenuation model and the noise model.

3.1 Transmission model

Deep space optical communication mainly takes atmosphere and free space as the transmission medium. The effects of atmospheric channel are similar to microwave communication in near Earth link, which includes two parts: atmospheric attenuation and turbulence effect.

- **Atmospheric attenuation.** When optical signal passes through the atmosphere, the molecules and other substances will make an absorption and scattering on it. Different wavelengths correspond to different atmospheric absorption conditions, which is shown in Figure 3-2 in [42].

It can be seen from the figure that atmospheric molecules absorb weakly only in several areas, which is called “atmospheric window”. Usually we choose an appropriate working wavelength to minimize the impact of atmospheric absorption and in actual channel modeling we only consider the impact of aerosols. Atmospheric aerosol is some large diameter particles which can generate Mie scattering on optical signal. The scattering coefficient is related to the density of particles in the atmosphere. The scattering coefficient increases with increasing density. The attenuation can be obtained by the following formula:

$$L = 10\lg[\exp(-kZm(\theta))] = -\frac{10kZm(\theta)}{\ln 10} \quad (\text{dB}), \quad (12)$$

where k is the attenuation coefficient of aerosols, Z is the transmission distance in atmosphere, θ is the Zenith angle, and $m(\theta)$ is the relative atmospheric mass along the zenith angle.

- **Turbulence effect.** Turbulence effect means the atmospheric refractivity varies randomly as place and time change, and the impact on beam propagation changes with geographical location, height, weather conditions and season conditions greatly. In general the turbulence decreases with increasing height, and it is weak at night while rising rapidly as the Sun rises. The effect of turbulence on optical transmission is related to the beam diameter d_B and the turbulence size l . When the ratio is far less than 1, it will mainly cause beam bending. When the ratio is about 1, it will mainly cause random beam drift. When the ratio is greater than 1, it will cause intensity scintillation, phase fluctuation and beam expansion [43, 44]. Experiments show that intensity scintillation is very small, and beam drift can also be suppressed by selecting a wide beam in practical application. The main attenuation is caused by the expansion

$$L = 10\lg \frac{A}{S} = 20\lg \frac{D}{L\theta_s}, \quad (13)$$

where A and S are transmit and receive power, D is receiver aperture, L is the distance, and θ_s is launch angle.

3.2 Noise model

The noise in optical communication mainly comes from two types of background light. One is extended background light source, which exists in the whole background, mainly from sky, starlight and Earth’s reflected light. The other is pointolite. It mainly comes from the Sun and the planet’s radiation. The average received power of these two noise, P_1 and P_2 , can be calculated by the following equation [45, 46]:

$$P_1 = W(\lambda) \times A \times \Delta\lambda \times \Omega_{fv} \times T, \quad (14)$$

$$P_2 = W(\lambda) \times A \times \Delta\lambda \times T, \quad (15)$$

where A is the optical aperture area of the receiver, $\Delta\lambda$ is the bandwidth, Ω_{fv} is the receiver field of view ($\Omega_{fv} = \frac{\pi}{4}\theta_r^2$), T is the transmittance, and $W(\lambda)$ is radiation spectrum function which shows atmosphere influence on radiation intensity at different wavelengths. Figure 1 in [47] shows the solar radiation spectrum measured vertically in the ground plane by the climate literacy labs of Georgia State University, while the radiant intensity of other stars is much smaller than that of the Sun.

Based on the transmission model and the noise model and other factors such as Doppler shift, optical communication channel can be modeled. Since the main characteristic of optical channel is scattering, and an important nature of the scattering process is linear and the number of particles acting on the path is huge, according to the central limit theorem, the scattering component arriving at the receiver aperture obeys a Gaussian distribution [48].

Compared to traditional microwave communication, optical communication has higher bandwidth, narrower beam angle, lower cost and better confidentiality. Although the establishment of deep space optical communication model has been basically completed, there are still some uncertain factors such as solar radiation spectrum function which need further study, and interstellar link also need to be improved, in order to lay a good foundation for future optical communications.

4 Conclusion

This paper introduces channel models for deep space communications in different scenarios, and gives some simulation results for Mars exploration. In addition, current situation of optical channel is also briefly introduced. This review shows that although many researches have been carried out, channel models for deep space communications are still limited to the AWGN model and its deformation due to its particularity and the incompleteness of measurement data. Numerous factors have not been fully considered. Therefore, it is worthwhile of researching whether there is other realistic model for deep space communications. Moreover, the existing channel modeling is incomplete. Future work can be carried out in the channel model on the surface of planets such as Mars. And the channel resource allocation is worth studying. The research results will be beneficial to the further development of deep space exploration.

Acknowledgements This work was supported by National Natural Science Foundation of China (Grant Nos. 61671263, 61271265), and Tsinghua University Independent Scientific Research Project (Grant No. 20161080057).

References

- 1 Liu J X. Forward to the deep space: developing trend of TTC&DT technology. *Telecommun Eng*, 2006, 2: 1–8
- 2 Zhang Y F, Du J C, Xiao S. Analysis and simulations on characteristics of deep space channel model VPAWGN. *Space Electron Technol*, 2010, 7: 22–25
- 3 Bokulic R S, Moore W V. Near Earth asteroid rendezvous spacecraft solar conjunction experiment. *J Spacecr Rockets*, 1999, 36: 87–91
- 4 Woo R. Radial dependence of solar wind properties deduced from HELIOS 1/2 and pioneer 10/11 radio scattering observation. *Astrophys J*, 1978, 219: 727–739
- 5 Woo R, Yang F C, Ishimaru A. Structure of density fluctuations near the Sun deduced from Pioneer-6 spectral broadening measurements. *Astrophys J*, 1976, 210: 593–602
- 6 Morabito D D, Shambayati S, Finley S, et al. The Cassini May 2000 solar conjunction. *IEEE Trans Antenn Propag*, 2003, 51: 201–219
- 7 Bokulic R S, Flaherty M K E, Jensen J R, et al. The NEAR spacecraft RF telecommunications system. *Johns Hopkins APL Tech Digest*, 1998, 19: 213–219
- 8 Feria Y, Belongie M, Mcpheeters T, et al. Solar Scintillation Effects on Telecommunication Links at Ka-band and X-band. TDA Progress Report 42-129, 1997
- 9 Morabito D D. Solar Corona Amplitude Scintillation Modeling and Comparison to Measurements at X-band and Ka-band. IPN Progress Report 42-153, 2003

- 10 Liu Q, Mei J J, Yao Y L, et al. Analysis of deep space channel model characteristics and its simulation. *J Air Force Radar Acad*, 2012, 3: 181–184
- 11 Hu X B, Xu H T, Zhou X W. Research of transmission loss analysis in deep space communication. In: *Proceedings of International Conference on Cyberspace Technology*, Beijing, 2013. 380–383
- 12 Xu H T, Zhou X W. Ka-band satellite channel model in deep space relaying network. *Wirel Pers Commun*, 2014, 77: 881–888
- 13 Zhou H, Zheng H X, Xu D G. *Space Communication Technology*. Beijing: National Defense Industry Press, 2010. 271–280
- 14 Lu W Q, Pan C S. An analysis of the factors that may affect the electromagnetic wave propagation in the space communications. *Fire Control Command Control*, 2004, 21–24
- 15 Zhang G X, Zhang H. *Satellite Mobile Communication System*. Beijing: Posts and Telecom Press, 2001
- 16 Guo Y, Zhao W J. Research and implementation of the satellite channel two-state markov model under the cloudy and foggy weather. In: *Proceedings of the 5th International Conference on Information Engineering for Mechanics and Materials*. Berlin: Springer, 2015
- 17 Sun K, Hou X, Zhao Q. Channel modelling and performance analysis of the near space based on the DS signal system. In: *Proceedings of MATEC Web of Conferences*, Les Ulis, 2016
- 18 Perez-Fontan F, Castro M A V, Enjamio C, et al. Comparison of generative statistical models for the LMS channel. In: *Proceedings of the 55th Vehicular Technology Conference*, Birmingham, 2002. 871–875
- 19 Shen D Y, Cui Y N, Zhang A F, et al. A simple simulation method for nakagami fading channel. In: *Proceedings of International Conference on Microwave and Millimeter Wave Technology (ICMMT)*, Chengdu, 2010. 160–163
- 20 Biscarini M, Marzano F S, Montopoli M, et al. Weather effects mitigation at Ka-band by using radiometeorological model forecast in deep space downlinks. In: *Proceedings of the 9th European Conference on Antennas and Propagation*, Lisbon, 2015
- 21 Morabito D D. Solar coronar induced fluctuations on spacecraft signal amplitude observed during solar superior conjunctions of the Cassini spacecraft. *Radio Science*, 2016, 42: 1–16
- 22 Xue Y H, Chai Y, Liu N B, et al. Sky-wave OTHR ionospheric channel modeling. *Chinese J Radio Sci*, 2013, 28: 862–868
- 23 Morabito D D. Spectral broadening and phase scintillation measurements using interplanetary spacecraft radio links during the peak of solar cycle 23. *Radio Sci*, 2009, 44: 1–23
- 24 Wu T, Yan Y, Li Y C, et al. Deep space channel modeling and the analysis of wave propagation environment characteristics under solar scintillation. *Chinese J Radio Sci*, 2015, 30: 417–422
- 25 Morabito D D. Solar Corona Amplitude Scintillation Modeling and Comparison to Measurements at X-band and Ka-band. *PN Progress Report 42-153*, 2003
- 26 Morabito D D, Shambayati S, Butman S, et al. The 1998 Mars Global Surveyor Solar Corona Experiment. *TMO Progress Report 42-142*, 2000
- 27 Rao Q L. The link analyzation and design based on CCSDS for Mars probe TTC&C system. Dissertation for Master Degree. Shanghai: Shanghai Jiaotong University, 2012
- 28 Liu Z H. Ka band deep space communication channel modeling based on the exploration of Mars. Dissertation for Master Degree. Suzhou: Suzhou University, 2012
- 29 Morabito D D, Schratz B, Bruvold K, et al. The Mars Science Laboratory EDL Communications Brownout and Blackout at UHF. *IPN Progress Report 42-197*, 2014
- 30 Wood G E, Asmar S W, Rebold T A, et al. Mars Pathfinder Entry, Descent, and Landing Communications. *TDA Progress Report 42-131*, 1997
- 31 Esatorius E, Estabrook P, Wilson J, et al. Direct-to-Earth Communications and Signal Processing for Mars Exploration Rover Entry, Descent and Landing. *IPN Progress Report 42-153*, 2003
- 32 He G L, Zhan Y F, Zhang J Z, et al. Characterization of the dynamic effects of the reentry plasma sheath on electromagnetic wave propagation. *IEEE Trans Plasma Sci*, 2016, 44: 232–238
- 33 Zhang J Z, He G L, Bai P, et al. Characterization and performance evaluation of turbulent plasma sheath channel. *China Commun*, 2016, 13: 88–99
- 34 Zhang J Z, He G L, Bai P, et al. Dynamic channel modeling for communication through turbulent plasma sheath. In: *Proceedings of International Conference on Wireless Communications & Signal Processing*, Nanjing, 2015
- 35 He G L, Zhan Y F, Ge N, et al. Channel characterization and finite-state Markov channel modeling for time-varying plasma sheath surrounding hypersonic vehicles. *Prog Electrom Res*, 2014, 145: 299–308

- 36 Ma H J, Zhu X L. The latest progress of free space laser communications. *Laser Optoelectron Prog*, 2005, 42: 7–11
- 37 Wilson K E. Overview of the ground-to-orbit laser communication demonstration. *Proc SPIE*, 1997, 2990: 23–30
- 38 Chen C C. Overview of the optical communications demonstrator. *Proc SPIE*, 1994, 2123: 85–94
- 39 Ma J, Tan L Y. The progress and trend of researches of intersatellite optical communications. *Chinese J Space Sci*, 2000, 20: 128–136
- 40 Kim I I. Preliminary result of the STRV-2 satellite-to-ground lasercom experiment. *Proc SPIE*, 2000, 3932: 21–34
- 41 Ke S Y. The research of channel model in space laser communication. Wuhan: Huazhong University of Science & Technology, 2007
- 42 Boroson D M, Scozzafava J J, Murphy D V, et al. The lunar laser communications demonstration. In: *Proceedings of the 3rd IEEE International Conference on Space Mission Challenges for Information Technology (SMC-IT)*, Pasadena, 2009. 23–28
- 43 Zhu X, Kahn J. Performance bound for coded free-space optical communication through turbulence channel. *IEEE Trans Commun*, 2003, 51: 1233–1239
- 44 Rao R Z, Wang S P. Experimental study of spot dancing of laser beam in a turbulent atmosphere. *Chinese J Lasers*, 2000, 27: 1011–1015
- 45 Lu Y, Lin Y S. The simple method to calculate the atmosphere transmittance of infrared radiation. *Infrared Technol*, 2003, 25: 45–49
- 46 Fan W, Wang Y, Rao R Z. Wavelength band selection method for target detection based on character of atmosphere radiation. *Infrared Laser Eng*, 2005, 34: 177–182
- 47 Climate Literacy Labs of Georgia State University. Lab 5: global surface temperature. 2014. <http://sites.gsu.edu/geog1112/global-surface-temperature/>
- 48 Wu C J, Yan C X. Overview of space laser communication. *Chinese J Opt*, 2013, 6: 670–678